




Article

# Synthesis and Characterization of a Composite Anion Exchange Membrane for Water Electrolyzers (AEMWE)

Somayyeh Rakhshani<sup>1</sup>, Rodolfo Araneo<sup>1</sup> , Andrea Pucci<sup>2</sup> , Antonio Rinaldi<sup>3</sup> , Chiara Giuliani<sup>3</sup> and Alfonso Pozio<sup>3,\*</sup>

<sup>1</sup> Department of Astronautical, Electrical and Energy Engineering, University of Rome, Via Eudossiana 18, 00184 Rome, Italy

<sup>2</sup> Department of Chemistry and Industrial Chemistry, University of Pisa, Via Moruzzi 13, 56124 Pisa, Italy

<sup>3</sup> ENEA, C.R. Casaccia, Via Anguillarese 301, 00123 Rome, Italy

\* Correspondence: alfonso.pozio@enea.it

**Abstract:** Anion exchange membranes (AEM) have gained attention recently as a promising candidate for low-cost water electrolysis systems to produce hydrogen, linked with renewable energy resources as a sustainable alternative to fossil fuels. The development of potential materials for producing and analyzing AEM is an imperative step towards commercialization and plays a competitive role in the hydrogen production industry. In this article, we developed a composite anion exchange membrane prepared by activating a commercial support structure (Celgard<sup>®</sup> 3401) with a commercially available functional group (Fumion<sup>®</sup> FAA-3) through a phase-inversion process. Fourier-transform infrared spectroscopy (FTIR) and Scanning Electron Microscopy (SEM) analysis demonstrated the phase-inversion procedure as an effective methodology. Furthermore, the cell performance test result (with Celgard/Fumion) was very promising and even better in comparison with a commercial membrane commonly applied in alkaline electrolysis (Fumasep). We also developed a testing procedure for membrane performance evaluation during electrolysis which is very critical considering the effect of CO<sub>2</sub> absorption on membrane conductivity.

**Keywords:** anion exchange membrane; alkaline water electrolysis; membrane characterization



**Citation:** Rakhshani, S.; Araneo, R.; Pucci, A.; Rinaldi, A.; Giuliani, C.; Pozio, A. Synthesis and Characterization of a Composite Anion Exchange Membrane for Water Electrolyzers (AEMWE). *Membranes* **2023**, *13*, 109. <https://doi.org/10.3390/membranes13010109>

Academic Editor: Kyu Hwan Lee

Received: 23 December 2022

Revised: 5 January 2023

Accepted: 11 January 2023

Published: 14 January 2023



**Copyright:** © 2023 by the authors. Licensee MDPI, Basel, Switzerland. This article is an open access article distributed under the terms and conditions of the Creative Commons Attribution (CC BY) license (<https://creativecommons.org/licenses/by/4.0/>).

## 1. Introduction

As we face a major challenge in the energy and environment sectors, considering the anthropogenic climate change hypothesis, searching for alternative energy strategies has become critical for future world energy demands. Among the numerous alternative energy approaches, green hydrogen serves as a low-cost, easily available, and abundant energy source with zero emissions of carbonaceous species and can play a key role in the energy transition strategy toward a stable and green future as it has a significant role in several applications and industries [1,2]. At the same time, it should be taken into consideration that the footprint of hydrogen technologies depends on their production processes and energy sources [3]. From this point of view, water electrolysis is a very promising and desired approach because of its compatibility with different types of electricity generation [4,5]. The search for investigation of efficient and cost-effective anion exchange membrane electrolyzers have been given much attention due to their ability to offer the advantages of conventional alkaline electrolysis technology [6,7] while also addressing the issue of cost associated with proton exchange membranes (PEMs) by using non-platinum group metals as electrocatalysts [8].

The anion exchange membrane water electrolyzer (AEMWE) is a technology built in a stack with solid polymer membranes to provide high volumetric energy density and it is compatible with non-precious metal catalyst electrodes which results in cost reduction of hydrogen production. The main difference between alkaline water electrolysis (AWE), which is a well-developed and mature technology [9–11], and AEMWE is that the

diaphragm that separates two half-cells in the former technology, despite being permeable to ions between two sides of the system, is not conductive. The conductivity is provided by alkaline hydroxide filling a porous diaphragm, while in AEMWE, the polymeric membrane is non-porous and has intrinsic anionic conductivity [1,12–15]. It is worth mentioning that in contrast to PEM electrolyzers which use only polymer electrolytes, many AEMWEs use liquid electrolytes (e.g., KOH or  $K_2CO_3$  solutions) in addition to polymer electrolytes to improve reaction kinetics [16]. The liquid electrolyte increases the local pH at the catalyst–electrolyte interface, generating an additional electrochemical interface. Having addressed the major challenges associated with AWEs, AEMWEs have attracted increasing interest from industrial and academic researchers in recent years.

Numerous studies and several papers and reviews have been published on the development of alkaline membranes for different applications (electrodialysis, electrodialysis reversal, desalination, or electro-deionization [17,18]) and from different aspects (separate components, material, technology, and operational conditions [2,16,19–21]). Most of the membranes produced were optimized for chemically less-aggressive environments concerning the pH and the operating temperature. The literature concerning the synthesis of anion exchange membranes (AEM) regarding those that use a hydroxide exchange membrane specifically designed for the electrolysis of water is scarce. The main function of the anionic membrane in alkaline electrolyzers is to transport hydroxide ions from the cathode to the anode and to avoid the movement of electrons and crossover of the gases produced by the electrochemical reactions in the two compartments. These membranes should ideally have high  $OH^-$  conductivity, high chemical stability (alkaline, oxidative, and thermal stability), excellent mechanical properties under wet conditions and high differential pressures, and low gas permeability. Generally, such membranes consist of a polymeric backbone that is responsible for mechanical and thermal stability and that is modified by positively charged functional groups on their backbone or pendant side chains. These modifiers facilitate anion movement and are responsible for ion-exchange capacity, ion conductivity, and transport number, enabling a zero-gap configuration and differential pressure operation.

A variety of AEM backbones have been studied and developed so far, such as polystyrene [22,23], poly-phenylene oxide (PPO) [24,25], polysulfone [26] or fluorinated polymers [27–29], poly-ethylene-co-tetrafluoroethylene (ETFE) [30], polyetherimide (PEI) [31], polyvinyl alcohol (PVA) [32], poly-ether-ether ketone [33], poly(arylene ether ketone) [34], and poly-carbazole [35]. As well, the most extensively investigated functional groups are:  $-NH_3^+$ ,  $-RNH_2^+$ ,  $-R_2NH^+$ ,  $=R_2N^{2+}$ ,  $-R_3P^+$ ,  $-R_2S^+$ , quaternary ammonium salts (QA) [36,37], and tertiary amines (e.g., BTMA) [31,32]. The cycloaliphatic QAs show remarkable alkaline stability [38].

As investigated and reported [6,39,40], the major challenge of anion exchange membranes is their low chemical and thermal stability, since the backbone and the functional group both suffer from hydroxide-induced degradation under alkaline conditions [41]. The degradation of polymer backbones leads detrimentally to chain rift, decreases the molecular weight, and results in increased brittleness of the membrane, and this effect is prominent in the presence of aromatic ether groups. Therefore, aromatic ether groups, which are present in many cheap and easily accessible polymers such as PEEK, PESU, and polyphenylene oxide (PPO), should be avoided. Furthermore, anion exchange membranes suffer from lower ionic conductivity in comparison to PEMs (such as Nafion) due to the lower mobility of  $OH^-$  than that of  $H^+$ .

Currently, a few alkaline solid polymeric membranes have been commercialized, such as Fumasep<sup>®</sup>, Sustainion<sup>®</sup>, Aemion<sup>™</sup>, and Orion<sup>™</sup>, and their main characteristics are summarized in Table 1 [2,39]. Membranes with different backbone materials show different conductivity, as shown in Table 1. The last three have a very high value with respect to Fumasep<sup>®</sup>, but it should be kept in mind that Fumasep is activated in  $Cl^-$  form, which has inferior mobility to that of  $OH^-$  [42], with a significantly higher thickness. There are very sporadic literature data on the usage of these membranes, and many were obtained

with unequal activation procedures or ionomer material, cell components, operational conditions, and even time periods of the cell performance tests, which makes a comparative study very difficult. The most-used membrane that has shown stable performance in AEMWE [1,43] is Fumasep, which we used as reference material in this article.

**Table 1.** Commercial AEM characteristics.

Brand Name	Company Country	Product Code	Material	Thickness	IEC (meq/g)	Conductivity (mS cm <sup>-1</sup> )	Refs.
Fumasep®	Fumatech (Germany)	FAA-3-PK-130	PK reinforced	130	1.1–1.4	4.0–8.0 (Cl <sup>-</sup> )	Data sheet
Sustainion®	Dioxide Material (USA)	37–50	Styrene based	50	-	70, 80 (OH <sup>-</sup> )	[14,44]
Aemion™	Ionomer Innovation Co. (Canada)	AF1-HNN8- AF1-HNN5-	HMT-PMBI * [45]	50 50	2.1–2.5 1.4–1.7	80 (OH <sup>-</sup> ) 15–25 (OH <sup>-</sup> )	Data sheet Data sheet
Orion™	Orion Polymer (USA)	Orion TM1™	Polyphenylene [46]	30	2.1	60 (OH <sup>-</sup> )	Data sheet

\* HMT-PMBI: hexamethyl-*p*-terphenyl poly (bibenzimidazolium).

The activation of porous support with desirable mechanical characteristics is a very simple approach to synthesizing anionic membranes. The performance of the membrane is then profoundly influenced by the supporting structure and the ionomer coupled together, so investigating the material and techniques to fabricate the backbone and activate it with different ionomers is a very interesting approach to developing AEMs. A supporting structure that can be used for this purpose is Celgard®, a typical polypropylene (PP) microporous membrane separator that is recognized for use in batteries [47,48]. PP is a low-cost polymer that is widely used for microporous membrane fabrication globally because of significant properties such as good thermal and mechanical stability and high resistance to extreme pH conditions [43,44]. Due to its numerous manufacturing applications and the huge amount of PP used globally, much research has been conducted on the sustainable assessment of PP production and recycling recently [49]. In the past, Stano et al. [50] used Celgard 2400 membranes modified with graft polymerization of acrylic acid after plasma activation in the conventional liquid alkaline electrolyzer. Tsehaye et al. [51] used Celgard 3501 impregnated with a commercial anion exchange ionomer (Fumion) to modify the support membrane to use as a separator in a Zn–air battery.

In this work, a composite anion exchange membrane was prepared by activating a porous support of commercial Celgard 3401 with an ionomer solution in a phase-inversion process. Phase inversion is an established technique commonly used for preparing membrane nano/microstructures. It is referred to as a chemical process in which a polymer is transformed from a liquid state to a solid state [48,52]. We used the commercially available ionomer solution Fumion (Fumatech Co., Bietigheim-Bissingen, Germany) with a QA functional group. The chemical structure of the Fumion polymer has not been disclosed; however it is reported [53] to contain a polyaromatic polymer with quaternary ammonium functional groups. The composite membrane was synthesized, characterized, and successively tested in a small lab electrolyzer to evaluate its performance. With the promising results revealed, we approach the challenge of fabricating porous substrates with controlled properties and a desired structure using low-cost polymeric materials with a highly efficient method to provide a robust, reproducible backbone for AEM in the future.

## 2. Experimental Procedures

### 2.1. Preparation of the Composite Anion Exchange Membranes

The composite anionic membrane reported here was prepared using a microporous monolayer membrane made of polypropylene with 41% porosity and 25 µm thickness, with surfactant-coated Celgard (Celgard®, Charlotte, CA, USA) to improve its hydrophilicity as the backbone, and was activated with Fumion FAA-3 solution in NMP 10% (Fumatech, Bietigheim-Bissingen, Germany). Activation was undertaken to ensure ion-exchange capacity and hydroxide conductivity for AEM applications. We carried out

the activation on small pieces of porous Celgard (4 cm × 4 cm). Our application relies on phase inversion, which involves the polymer transforming from the liquid phase of the solution into the solid phase. The concept of the phase-inversion process has been explained elsewhere [52]. Phase inversion can be induced with different techniques, such as immersion precipitation, precipitation by controlled evaporation, thermal precipitation, or vapor-phase precipitation. The choice of method of phase inversion is highly dependent on the type of polymer and the solvent used to dissolve the polymer. As the first approach, we decided to use immersion precipitation by customizing it into a manual batch mode, applying a certain amount of ionomer solution and inversion solution. For each piece of the sample, we dropped 0.5 mL of Fumion FAA-3 solution on the membrane surface until it became transparent, and then we did the same on the other side of the membrane. After 10 min, we dropped 0.5 mL of toluene—as a non-solvent to induce inversion—on the Celgard surface. After 10 min, we repeated the operation on the other side of the membrane. Then we let it dry at room temperature overnight under the hood (Figure 1).

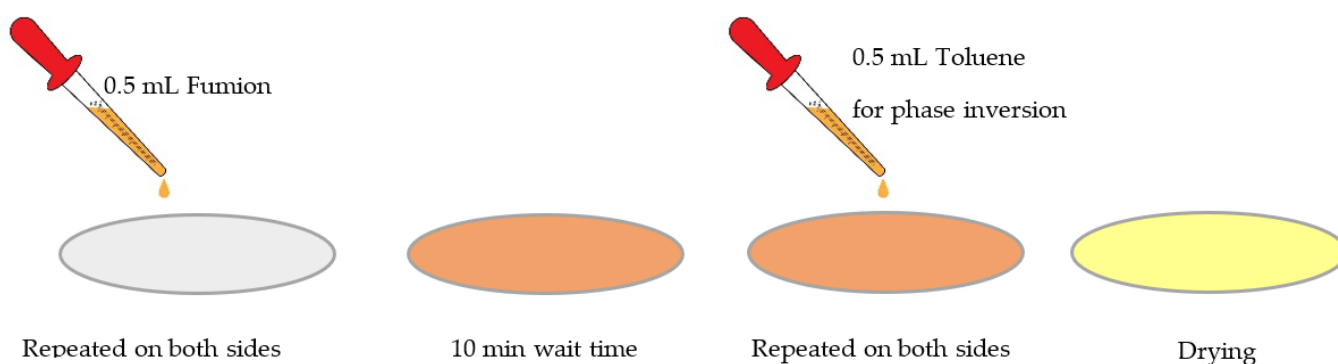


**Figure 1.** Schematic of membrane activation procedure in the phase-inversion method.

## 2.2. Characterization

### 2.2.1. Physical Chemical Analysis

Fourier Transform Infrared (FTIR) spectra of dried samples were collected in the wave number range 400–3500  $\text{cm}^{-1}$  using a Nicolet iS5 FT-IR spectrometer (Thermo Fisher Scientific, Waltham, MA, USA) equipped with an attenuated total reflectance (ATR) accessory. The measurements were recorded using a diamond crystal cell ATR, typically using 32 scans at a resolution of 4  $\text{cm}^{-1}$ . The samples were all measured under the same mechanical force pushing the samples into contact with the diamond crystal. No ATR correction has been applied to the data. SEM morphological characterization was acquired with a field-emission gun scanning electron microscope (ZEISS, Jena, Germany). The air permeability measurement of the membrane after activation with Fumion was performed with a Gurley 4320 densitometer (Rycobel, Deerlijk, Belgium) as described elsewhere [54].

### 2.2.2. Ionic Exchange Capacity (IEC)

The IEC of an ion-exchange membrane (IEM) is an analytical parameter that represents the ability of ionic transfer within an alkaline solid polymeric membrane and is significantly influenced by the ion conductivity of the membrane [3]. It is measured when the counterions are  $\text{OH}^-$  using a titration method and it is expressed as milliequivalent per gram of the dry membrane ( $\text{meq g}^{-1}$  dry IEM). The method is well-described elsewhere [55]. Briefly, the membrane was converted into  $\text{OH}^-$  form by immersing it in 100 mL 1M KOH and 2 days. Then the membrane was washed and immersed in 100 mL of a 0.01 HCl solution for 24 h and finally we measured IEC using back titration. The  $\text{OH}^-$  content in the membrane was calculated using the following equation:

$$IEC = \frac{n_{\text{HCL},i} - n_{\text{HCL},f}}{m} \quad (1)$$

where  $n_{HCl,i}$  is the amount of HCl in the initial solution (0.01 M, 100 mL),  $n_{HCl,f}$  is the amount of HCl in the final solution after neutralization of the membrane, and  $m$  is the dry membrane mass. Attention must be placed in this characterization that could be affected in some step by the accumulation of carbonate and bicarbonate ions with an underestimation of the final value of IEC.

### 2.2.3. Ionic Conductivity

The membrane conductivity can be obtained from the measurement of the resistivity of the membrane against the flow of current using a four-point probe electrochemical cell (Figure 2). The method is explained elsewhere [55]. Briefly, the cell is composed of two compartments that can house membranes with a diameter of 3.5 cm with an area exposed to the solution equal to 7.07 cm<sup>2</sup>. The ionic conductivity of the membrane was determined with at least three successive measurements of the potential difference between the reference electrodes. A linear voltage sweep was applied in short time intervals (5 s), voltage vs. current was plotted, and the slope gives us the resistance ( $\Omega$ ) without the membrane and with the membrane between the two compartments. For this experiment, the NaCl solution in the cell was maintained at 0.5 M. Without the membrane, the measured resistance of the aqueous NaCl solution between the two reference electrodes is  $R_{cell}$ ; with a membrane, the total resistance is the sum of the resistance of the cell and that of the membrane:  $R_{measure} = R_{membrane} + R_{Cell}$ . Knowing the cell resistance ( $R_{cell}$ ), the value of the membrane resistance is defined as the difference between these two resistances:  $R_{membrane} = R_{measure} - R_{Cell}$ . The ionic conductivity,  $\sigma$  (S cm<sup>-1</sup>), of the membrane can be determined using the following relationship:

$$\sigma = \frac{1}{R_{membrane}} \frac{l}{S} \quad (2)$$

where  $l$  is the thickness of the membrane (cm),  $S$  is the surface area of the membrane exposed to the electric field (cm<sup>2</sup>), and  $R_{membrane}$  is the membrane resistance ( $\Omega$ ). The product  $R_{membrana} \times S$  represents the area-specific resistance (ASR).

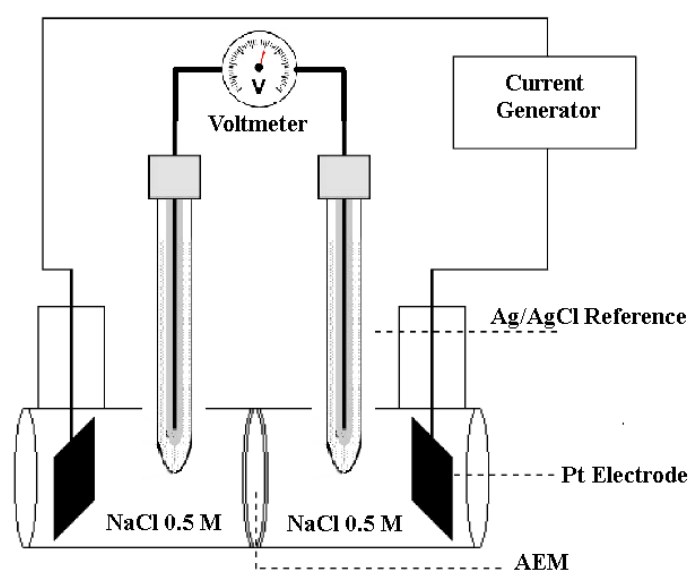


**Figure 2.** Schematic representation of experimental conductivity cell.

### 2.2.4. Electrochemical Performance

The electrochemical performance test of the membrane was carried out in a lab-scale 2 cm<sup>2</sup> electrolyzer (two-electrode) at room temperature with stainless steel gas diffusion electrodes (GDE). The cell (Figure 3) was made of steel on both the cathode and anode

sides. The GDE ( $\varnothing$  16 mm) that ensured the electrical contact of the anionic membrane and the diffusion of the water and gases produced was supplied by Bekaert Fiber Technologies (Belgium). It is a commercial matrix in sintered metal fiber in AISI 316-L steel with a thickness of 0.51 mm and with a porosity of 82% and compressibility of approx. 5.4%. The anodic side can be fed with distilled water or a KOH solution 0.5 M (in our case study the latter was the choice), contained in a 500 mL polyethylene tank using a metering pump (KMS), in PTFE with a flow of  $100 \text{ mL min}^{-1}$ . The cathode side output can be connected to a volumetric system for measuring the hydrogen produced.

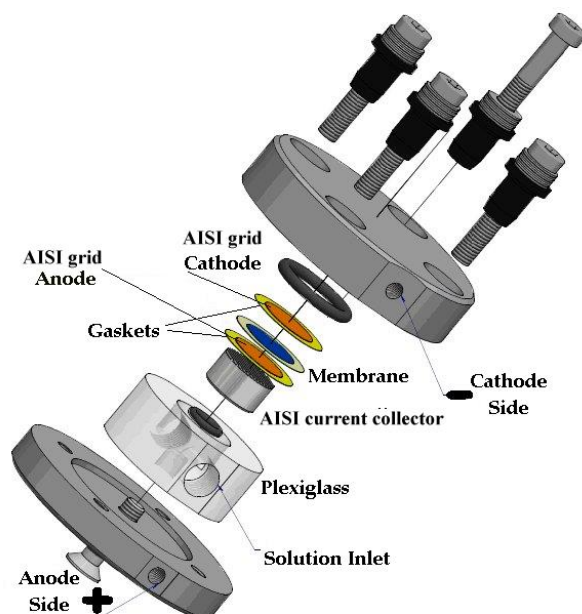


Figure 3. Experimental cell for electrochemical measurement.

The cell was connected to a Solartron Mod. 1287 potentiostat/galvanostat and a Solartron Mod. 1260 frequency response analyzer, both interfaced with a GPIB card to a personal computer. Electrochemical impedance spectroscopy (EIS) measurements were performed in the 1 MHz–1 Hz frequency range at open circuit potential (OCP); the amplitude of the AC signal was always  $10 \text{ mV}_{pp}$ . Both static and dynamic galvanic polarization were performed in the same cell configuration as the EIS measurements. The characteristic E vs. I curves were also recorded on the cell at room temperature ( $298 \text{ K}$ ) in the current range of  $0\text{--}1000 \text{ mA cm}^{-2}$ . Graphs of cell voltage versus time were recorded continuously and impedance spectra were periodically acquired at the OCP.

EIS is a quantity that measures the opposition of a system to the passage of current and in DC conditions, coincides with the resistance value. It is also a “transient” technique, in the sense that, when one of the quantities that determine the state of the system is perturbed, relaxation to a new steady state occurs with a speed dependent on the parameters (kinetics, transport, etc.) of the system.

The impedance spectra can be represented with Nyquist diagrams, in which the high-frequency intercept ( $R_{HF}$ ) represents the ohmic resistance of the system, while the diameter of the semicircle is basically related to the polarization resistance sum of various contributions (diffusion, charge transfer).

The measurements were conducted on the electrolysis cell shown in Figure 3 in a flow of 0.5 M KOH at a temperature of  $25 \text{ }^\circ\text{C}$ . The measured resistance value  $R_{HF}$  is that relating to the high-frequency resistance, i.e., the intercept with the  $Z_{Re}$  axis by  $Z_{Imm} = 0$  in the Nyquist diagram. Once the value is known, it is possible to calculate the specific resistance  $R_\Omega$  ( $\Omega \text{ cm}^2$ ) for the cell:

$$R_\Omega = R_{HF} \times S \quad (3)$$

where  $S$  is the surface area of the membrane ( $2.0 \text{ cm}^2$ ) in the electrolyzer. This measurement also allows estimation of the intrinsic conductivity of the membrane (i.e., the conductivity induced by counter ions associated with positive ionic sites of the ionomer and favoured by water molecules).

### 3. Results and Discussion

#### 3.1. FTIR and SEM Membrane Analysis

The FTIR analysis confirms the success of the Celgard activation with the ionomer solution by applying the proposed procedure. FTIR spectra of the Celgard samples before and after the Fumion activation are reported in Figure 4. Fumion (ionomer solution in NMP solvent) and NMP are also reported for clarity. Fumasep PK-130, in the  $\text{Br}^-$  and  $\text{OH}^-$  form, is used as a reference. Chemically, the Fumion ionomer is a polyaromatic polymer with ether bonds in the main chain and quaternary ammonium groups attached to the main chain (Figure 4b). The spectrum of the membrane after the ionomer activation (Celgard/Fumion) shows the presence of some peaks due to the ionomer. In particular, it is possible to observe the infrared absorption at  $1671 \text{ cm}^{-1}$ , due to the  $=\text{CH}_2$  bending vibration from the aromatic rings, and at  $1602 \text{ cm}^{-1}$ , attributable to the stretching vibration of the N-C groups from the quaternary ammonium groups. In addition, the peak at  $1187 \text{ cm}^{-1}$  is detected in both the Celgard/Fumion (intense peak) and Fumion spectra (weak peak). This infrared absorption is not present in the NMP spectrum. This evidence suggests that the peak is probably due to the polymer dissolved in the ionomer solution. It is worth noting that the FTIR spectrum of Celgard activated with Fumion is comparable to that of the commercial membrane Fumasep, selected as the reference.

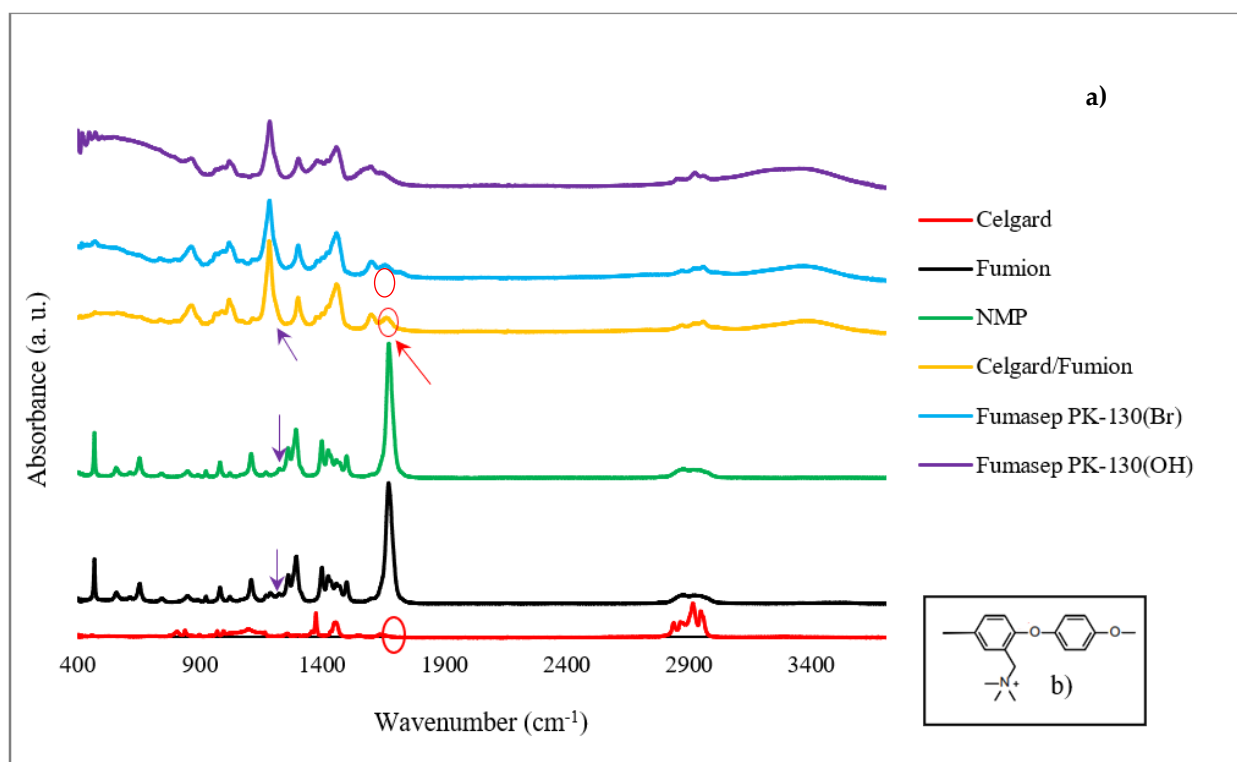


**Figure 4.** (a) FTIR spectrum of the Celgard before and after activation, Fumion, Fumasep PK-130 (in  $\text{Br}^-$  and  $\text{OH}^-$  form), and NMP solvent, (b) chemical structure of Fumion.

The Celgard support consists of intertwined fibers with a porosity of about 41% and a variable pore size on the order of microns or smaller (Figure 5a). As visible in Figure 5b, after activation, the Fumion ionomer filled the pores, and we can see they are aligned

along the pores' locations which confirms the presence of the functional QA group in our composite membrane.

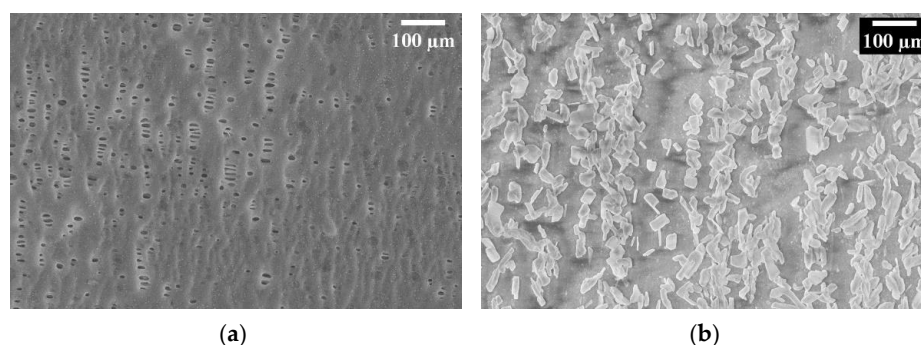


**Figure 5.** SEM image of Celgard 3401, (a) before activation (b) after activation with Fumion.

The permeability measurements on the activated Celgard support, which had a Gurly number of 620 s initially, were infinite time after activation with Fumion. This means the pores had been filled with Fumion. Furthermore, it was subsequently put in the conductivity measurement cell in which one side of the activated membrane was filled with the solution and left overnight. No solution passed through the membrane to the other side, indicating that there were no pores left inside the membrane. Further analysis is necessary to better evaluate how the pore volume and porosity of the substrate affect the membrane's properties, and their correlation with phase inversion results.

### 3.2. Ion-Exchange Capacity and Ionic Conductivity Measurement

Figure 6 shows the voltage–current measurement on Fumasep-PK-130 and Celgard/Fumion membranes. The slope is greater for Fumasep, indicating a higher resistance due to its thickness. Table 2 shows the calculated conductivity for both membranes using Equation (2), obtained by measuring  $K_{\text{cell}}$  and  $R_{\text{cell}}$  in a NaCl 0.5 M solution at 25 °C (respectively,  $K_{\text{cell}} = 369.39 \text{ cm}^{-1}$ ,  $R_{\text{cell}} = 0.038 \text{ } \Omega$ ). The conductivity of the commercial Fumasep is within the ranges provided by the producer in the datasheet for the  $\text{Cl}^-$  form ( $4\text{--}8 \text{ mS cm}^{-1}$ ). Table 2 also reports IEC defined using titration for the samples. Despite the composite membrane having lower conductivity and IEC than the commercial one, the ASR is lower due to its minor thickness. This result represents a good compromise where poor ion conductivity could be compensated for with a low area-specific resistance (ASR).

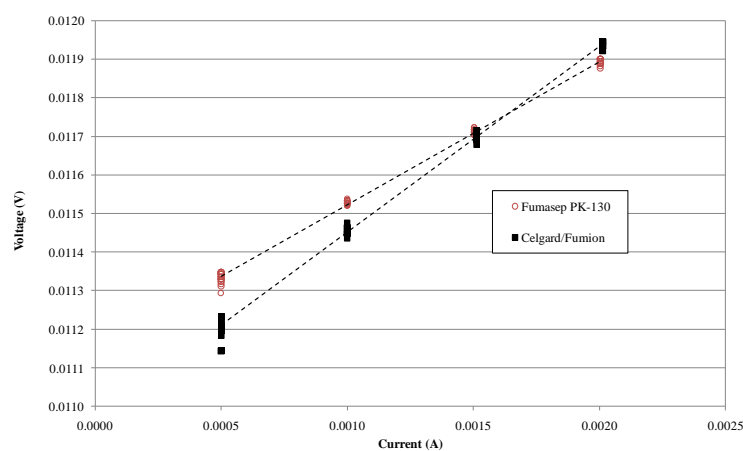


**Figure 6.** Voltage vs. current measurement on Fumasep-PK-130 (○) and Celgard/Fumion (■) membrane in NaCl 0.5 M at 25 °C.



**Table 2.** IEC and conductivity of sample membranes.

Membrane	Thickness ( $\mu$ )	IEC ( $\text{meq g}^{-1}$ )	$R_{\text{measure}}$ ( $\Omega$ )	$R_{\text{membrane}}$ ( $\Omega$ )	ASR ( $\Omega \text{ cm}^2$ )	$\sigma_{\text{membrane}}$ ( $\text{mS cm}^{-1}$ )
Celgard/Fumion	25	0.44	0.22	0.19	1.3	$3.0 \pm 0.1$
Fumasep PK-130	130	1.29	0.36	0.32	2.3	$5.7 \pm 0.2$

### 3.3. Electrochemical Characterization of Membranes

To evaluate membrane functionality, long-term electrolysis tests were carried out on both membranes to allow comparison.

Figure 7 shows the electrolysis voltage of the two cells at a current density of  $50 \text{ mA cm}^{-2}$  during the first 163 h of operation. Both membranes exhibit a voltage between 2 and 2.1 V and over time reach a value of about 2.05 V. However, a substantial difference is observed during the initial phase (the first 20 h) while the membranes were pre-treated the same way (approximately 24 h in KOH 0.5 M). As illustrated in the inside figure of Figure 7 the commercial Fumasep membrane cannot immediately maintain the electrolysis current set at  $50 \text{ mA cm}^{-2}$  and so it is necessary to reduce the initial current value to  $12.5 \text{ mA cm}^{-2}$  and then progressively increase it to 25 and finally to  $50 \text{ mA cm}^{-2}$ . The behavior appears to be closely related to the conductivity of the membrane, which at first does not provide adequate transport of  $\text{OH}^-$  ions inside, more likely due to the formation of larger, less mobile ions ( $\text{CO}_3^{2-}$  and  $\text{HCO}_3^-$ ) due to the carbonation of the membrane.

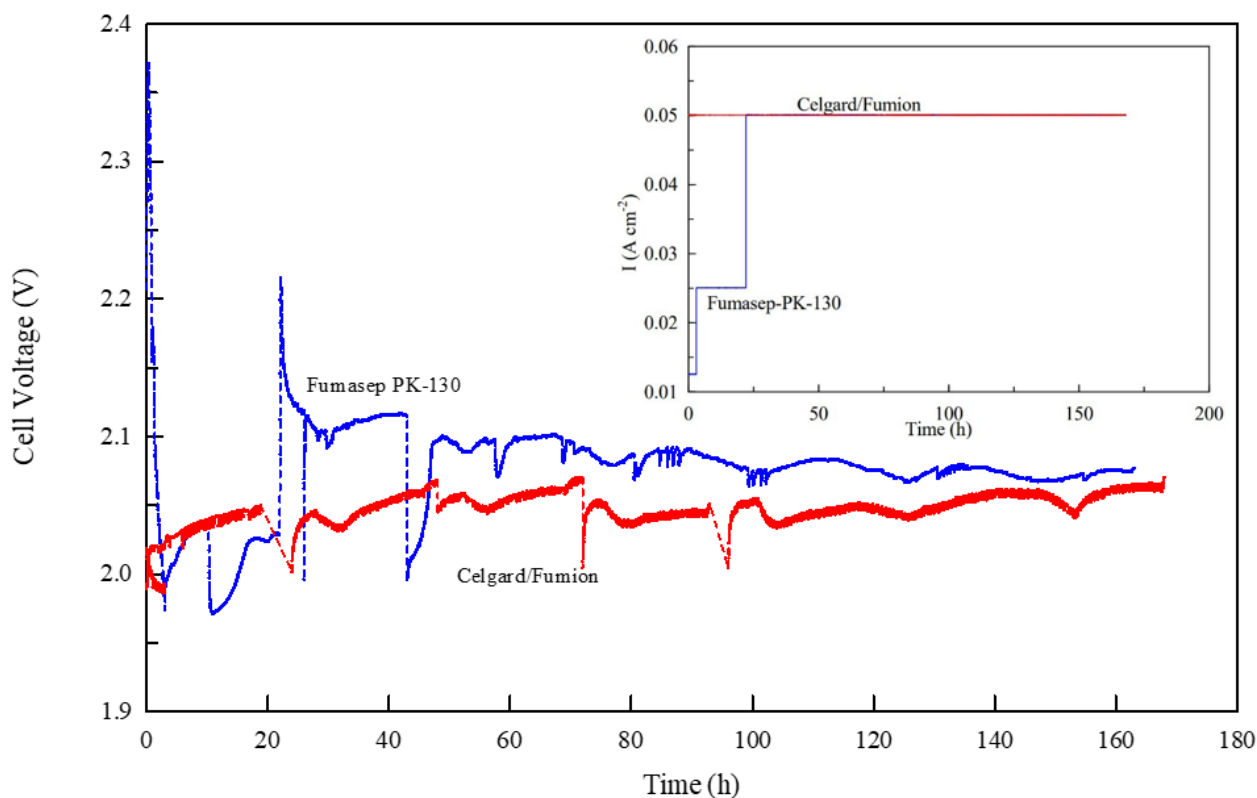
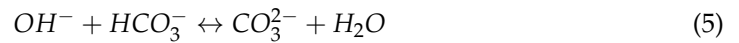


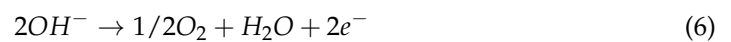
**Figure 7.** Measurement of cell voltage vs. time for Celgard/Fumion and Fumasep-PK-130 membranes at 25 °C. The inset figure shows the current density profile during the experiment.

This is explained by the fact that AEM is very reactive to  $\text{CO}_2$  in the environment. In an AEMWE, hydroxide anions ( $\text{OH}^-$ ) are responsible for creating current as they are transported through the anion exchange membrane (AEM) from the cathode to the anode side of the cell. However, upon exposure to the ambient air which contained  $\text{CO}_2$ , the carbonation process takes place very fast following the chemical reactions (4) and (5) so

that the accumulation of bicarbonate ions on the membrane interface confines the mass transport of  $\text{OH}^-$  ions at the cathode. Thus, hydroxide concentration in the membrane decreases and negatively affects cell performance [56–58].



This effect appears to be detrimental for several reasons: (1) The membrane is normally produced in chloride or bromide form and changed to  $\text{OH}^-$  form before insertion into the cell by immersion in an alkaline solution. (2) The carbonation process depends on the air-exposure time of the membrane after treatment with hydroxide and heavily influences its conductivity and electrolysis performance. (3) Over time the level of  $\text{CO}_2$  contamination of the circulating solution can vary, especially if the cell remains inactive for a long time. In the literature, methods have been reported for the de-carbonation of membranes before ex situ conductivity measurement. As an example, Kimura et al. [56] tested an activation procedure in a closed system with a  $\text{CO}_2$ -free atmosphere using nitrogen-treated water. Ziv et al. [57] electrochemically purged the carbonate ions in the membrane by applying an electrolysis current in a humidified and  $\text{CO}_2$ -free atmosphere for one week. In this way, the oxygen generated at the anode (6) replaces the  $\text{CO}_2$  and the hydroxide generated at the cathode replaces the carbonate ions by shifting reaction (4) to the left over time.



These studies show that to verify the performance of an anionic membrane, it is necessary to achieve a prolonged pre-treatment phase of electrolysis with a gradual increase in current to eliminate  $\text{CO}_2$ . In our study, both membranes showed the same carbonation effect in electrolysis (Figure 7). Figures 8 and 9 show the voltage vs. current density after the different electrolysis times shown in Figure 7. The electrolysis at constant current density was stopped after various time intervals and a Galvano-dynamic experiment was performed at  $1 \text{ mAs}^{-1}$ . Initially, the electrolyzer's current density is constrained by the conductivity drop due to the accumulation of carbonate and bicarbonate ions, which inhibit the transport of  $\text{OH}^-$  ions. Following Figures 8 and 9, both systems reached a higher maximum current density as electrolysis proceeded but with different values. A minimum amount of current and gas evolution (reactions 6 and 7) allows the elimination of carbonate ions and the recovery of the  $\text{OH}^-$  conductivity resulting in an increase in the electrolysis current. However, the maximum current density achievable by the system progressively increases with the working hours of the electrolysis test. The same behavior of current limitation due to the  $\text{CO}_2$  effect was studied in detail by Ziv et al. in anion exchange membrane fuel cells (AEMFCs) and is well illustrated in references [57,58].

As follows from the voltage–current density plot, at zero time the cell with the Celgard/Fumion membrane reaches a maximum current density of  $569 \text{ mA cm}^{-2}$  while after 163 h of electrolysis the maximum current reaches  $933 \text{ mA cm}^{-2}$ . The cell with Fumasep membrane also shows similar behavior, with  $57 \text{ mA cm}^{-2}$  at zero time and  $740 \text{ mA cm}^{-2}$  after 163 h. For both cells, the presence of a limiting effect due to hydroxide transport appears in the first working hours. However, the time expansion is more noticeable for the commercial membrane, whose recovery time is longer, likely due to its higher thickness. The results also indicate that thinner membranes are preferred since they react more rapidly to the de-carbonation process during electrolysis.

The results revealed that measuring membrane performance in a small electrolysis cell is very challenging, and to make a reliable comparison between different membranes requires long-term electrolysis. Furthermore, preparation using phase inversion is a fast and easily applicable method for synthesizing composite membranes with different backbone structures and ionomer solutions.

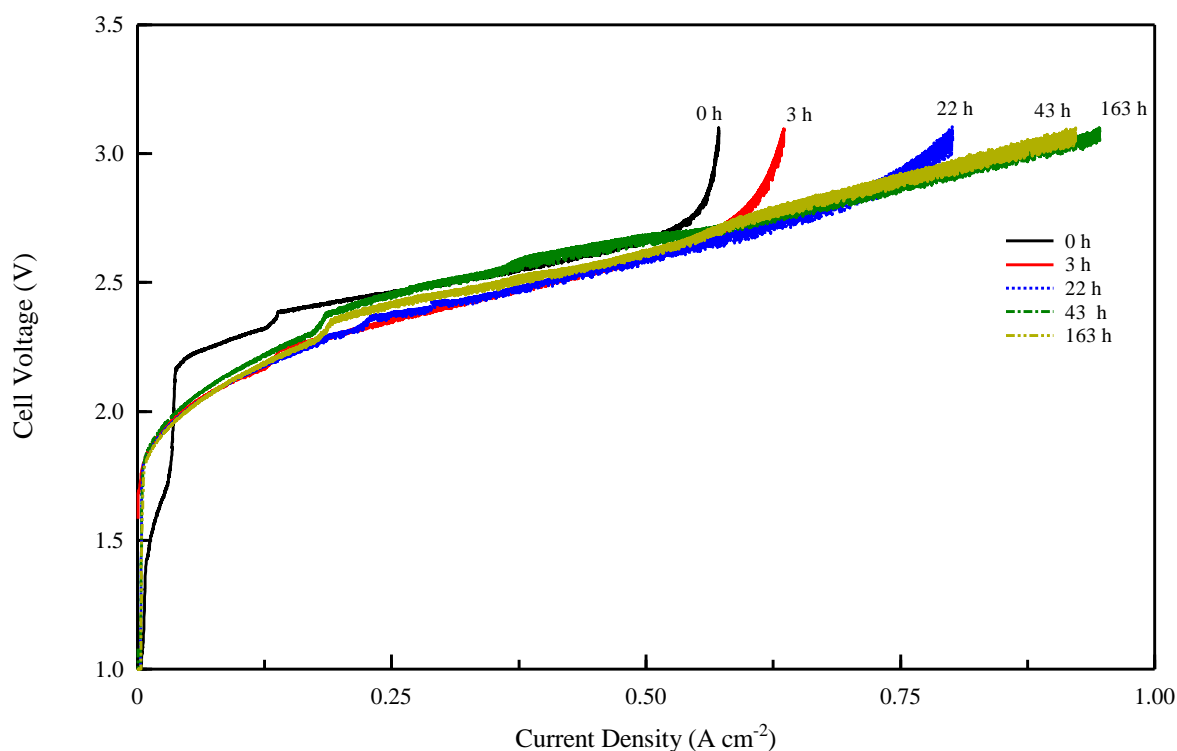


**Figure 8.** Cell voltage vs. current density profile for Celgard/Fumion membrane after different electrolysis times at 25 °C.

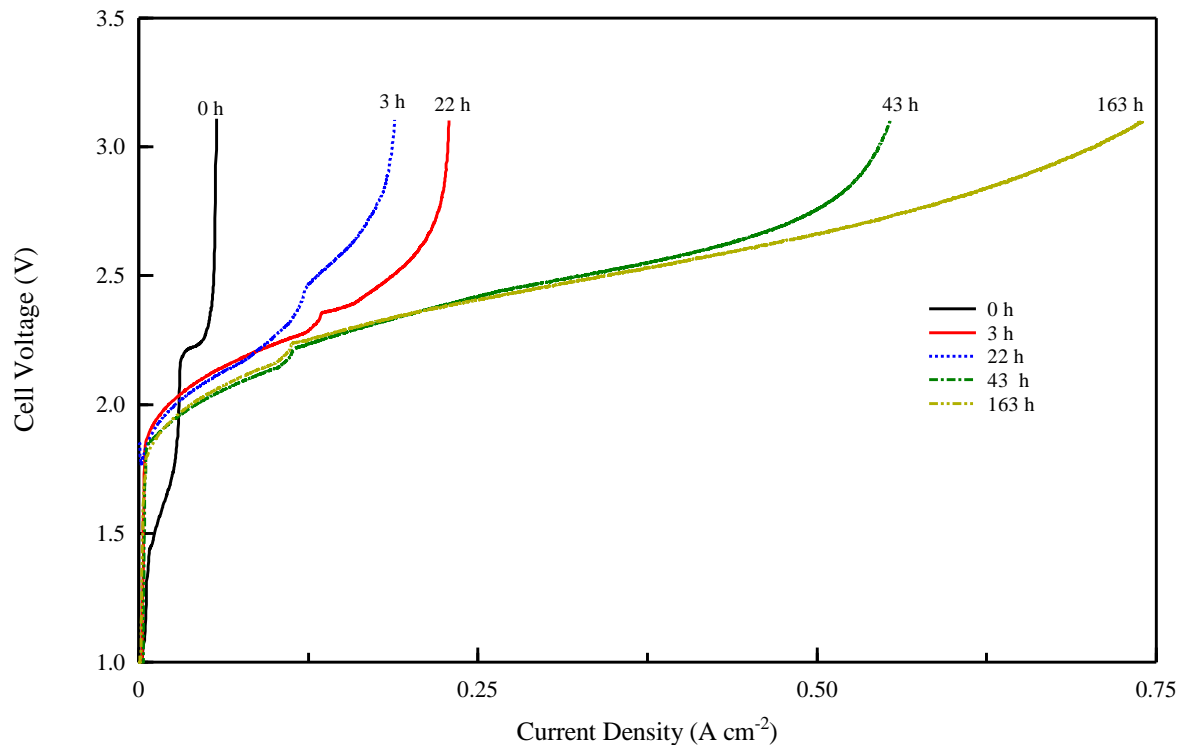


**Figure 9.** Cell voltage vs. current density profile for Fumasep-PK-130 membrane after different electrolysis times at 25 °C.

Continuing the measurements, the commercial Fumasep membrane did not reach the same performance as the Celgard/Fumion, even after the electrolysis test was prolonged up to 310 h (Figures 10 and 11).

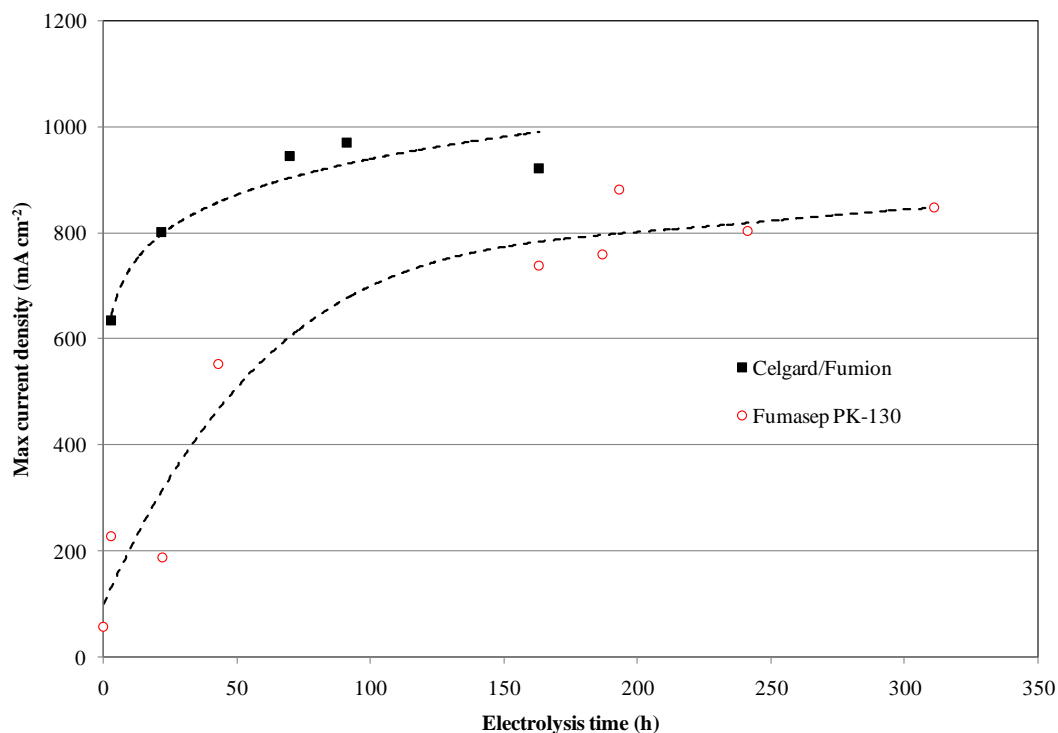


**Figure 10.** Maximum current density profile at 3.1 V vs. time on Fumasep-PK-130 and Celgard/Fumion at 25 °C.

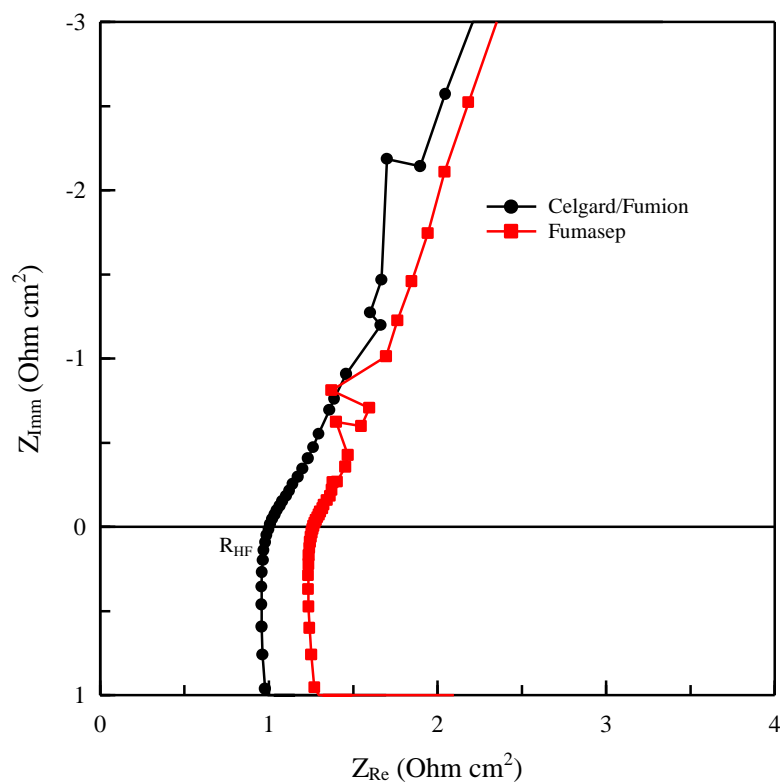


**Figure 11.** Nyquist plot for cell with Fumasep and Celgard/Fumion membranes at 25 °C and OCP (in electrochemical impedance spectroscopy—EIS).

Further insight into the membranes is provided by the impedance analysis of the two cells in hydroxide form during the electrolysis test. The conductivity value calcu-

lated from cell impedance spectroscopy has an average value of  $5 \pm 1 \text{ mScm}^{-1}$  for Celgard/Fumion while it is  $9 \pm 1 \text{ mScm}^{-1}$  for Fumasep. The in situ measurements confirm that despite the lower conductivity of our composite membrane, from an electrochemical standpoint it is more efficient thanks to the lower specific resistance due to its lower thickness. It also seems that the thickness of the membrane influences the time needed for activation of the membrane. The thinner the membrane is, the shorter the time needed for releasing carbonate ions, as observed for the composite membrane (Celgard/Fumion).

#### 4. Conclusions

A composite anion exchange membrane was synthesized by applying commercial material—support structure Celgard 3401 and commercially available functional group Fumion FAA-3—through a phase-inversion process and successfully tested in an electrochemical cell. The success of phase inversion as a method of activation was demonstrated with FTIR and SEM analysis. This study showed that the composite membrane has a higher maximum current density than the Fumasep membrane. This implies better performance and supports the validity of this practice as a potential approach for fast production and characterization of AEMs which needs further optimization. In this regard, the idea of producing porous substrates with controlled rheological properties and desired structure out of low-cost polymeric material with an efficient technique to provide a robust, reproducible backbone for AEM stands out.

Moreover, we evaluated and developed a testing protocol for membrane performance during electrolysis, which is very relevant, considering the effect of  $\text{CO}_2$  absorption on conductivity, to create a reliable inter-laboratory comparison. The absence of a well-established international cell performance test protocol, however, seems to be a profound hurdle to enable researchers to make a solid comparison with literature results.

**Author Contributions:** Conceptualization, A.P. (Alfonso Pozio) and S.R.; methodology, A.P. (Alfonso Pozio), A.P. (Andrea Pucci); validation, A.P. (Alfonso Pozio), A.P. (Andrea Pucci), R.A. and A.R.; formal analysis, A.P. (Alfonso Pozio), A.P. (Andrea Pucci), A.R. and R.A.; investigation, S.R., A.P. (Alfonso Pozio) and C.G.; resources, A.P. (Alfonso Pozio); data curation, S.R., A.R., C.G. and A.P. (Alfonso Pozio); writing—original draft preparation, A.P. (Alfonso Pozio), S.R. and C.G.; writing—review and editing, A.P. (Alfonso Pozio) and S.R.; supervision, A.P. (Alfonso Pozio); project administration, A.P. (Alfonso Pozio); funding acquisition, A.P. (Alfonso Pozio). All authors have read and agreed to the published version of the manuscript.

**Funding:** This research was funded by Italian MISE, IEMAP project.

**Institutional Review Board Statement:** Not applicable.

**Data Availability Statement:** The data presented in this study are available on request from the corresponding author.

**Conflicts of Interest:** The authors declare no conflict of interest.

#### References

1. Vincent, I.; Bessarabov, D. Low cost hydrogen production by anion exchange membrane electrolysis: A review. *Renew. Sustain. Energy Rev.* **2018**, *81*, 1690–1704. [[CrossRef](#)]
2. López-Fernández, E.; Sacedón, C.G.; Gil-Rostra, J.; Yubero, F.; González-Elipse, A.R.; de Lucas-Consuegra, A. Recent Advances in Alkaline Exchange Membrane Water Electrolysis and Electrode Manufacturing. *Molecules* **2021**, *26*, 6326. [[CrossRef](#)] [[PubMed](#)]
3. Zakaria, Z.; Kamarudin, S.K. A review of alkaline solid polymer membrane in the application of AEM electrolyzer: Materials and characterization. *Int. J. Energy Res.* **2021**, *45*, 18337–18354. [[CrossRef](#)]
4. Wang, M.; Wang, Z.; Gong, X.; Guo, Z. The intensification technologies to water electrolysis for hydrogen production—A review. *Renew. Sustain. Energy Rev.* **2014**, *29*, 573–588. [[CrossRef](#)]
5. Matute, G.; Yusta, J.; Correas, L. Techno-economic modelling of water electrolyzers in the range of several MW to provide grid services while generating hydrogen for different applications: A case study in Spain applied to mobility with FCEVs. *Int. J. Hydrog. Energy* **2019**, *44*, 17431–17442. [[CrossRef](#)]

6. Miller, H.A.; Bouzek, K.; Hnat, J.; Loos, S.; Bernäcker, C.I.; Weissgaerber, T.; Röntzsch, L.; Meier-Haack, J. Green hydrogen from anion exchange membrane water electrolysis: A review of recent developments in critical materials and operating conditions. *Sustain. Energy Fuels* **2020**, *4*, 2114–2133. [[CrossRef](#)]
7. Kiaee, M.; Infield, D.; Cruden, A. Utilisation of alkaline electrolyzers in existing distribution networks to increase the amount of integrated wind capacity. *J. Energy Storage* **2018**, *16*, 8–20. [[CrossRef](#)]
8. Chisholm, G.; Cronin, L. *Hydrogen from Water Electrolysis*; Elsevier Inc.: Amsterdam, The Netherlands, 2016. [[CrossRef](#)]
9. Colli, A.N.; Girault, H.H.; Battistel, A. Non-Precious Electrodes for Practical Alkaline Water Electrolysis. *Materials* **2019**, *12*, 1336. [[CrossRef](#)] [[PubMed](#)]
10. Pérez-Alonso, F.; Adán, C.; Rojas, S.; Peña, M.; Fierro, J. Ni/Fe electrodes prepared by electrodeposition method over different substrates for oxygen evolution reaction in alkaline medium. *Int. J. Hydrog. Energy* **2014**, *39*, 5204–5212. [[CrossRef](#)]
11. Marini, S.; Salvi, P.; Nelli, P.; Pesenti, R.; Villa, M.; Berrettoni, M.; Zangari, G.; Kiros, Y. Advanced alkaline water electrolysis. *Electrochim. Acta* **2012**, *82*, 384–391. [[CrossRef](#)]
12. Santoro, C.; Lavacchi, A.; Mustarelli, P.; Di Noto, V.; Elbaz, L.; Dekel, D.R.; Jaouen, F. What is Next in Anion-Exchange Membrane Water Electrolyzers? Bottlenecks, Benefits, and Future. *Chemsuschem* **2022**, *15*. [[CrossRef](#)]
13. Motealleh, B.; Liu, Z.; Masel, R.I.; Sculley, J.P.; Ni, Z.R.; Meroueh, L. Next-generation anion exchange membrane water electrolyzers operating for commercially relevant lifetimes. *Int. J. Hydrog. Energy* **2021**, *46*, 3379–3386. [[CrossRef](#)]
14. Liu, Z.; Sajjad, S.D.; Gao, Y.; Yang, H.; Kaczur, J.J.; Masel, R.I. The effect of membrane on an alkaline water electrolyzer. *Int. J. Hydrog. Energy* **2017**, *42*, 29661–29665. [[CrossRef](#)]
15. Leng, Y.; Chen, G.; Mendoza, A.J.; Tighe, T.B.; Hickner, M.A.; Wang, C.-Y. Solid-State Water Electrolysis with an Alkaline Membrane. *J. Am. Chem. Soc.* **2012**, *134*, 9054–9057. [[CrossRef](#)]
16. Li, D.; Motz, A.R.; Bae, C.; Fujimoto, C.; Yang, G.; Zhang, F.-Y.; Ayers, K.E.; Kim, Y.S. Durability of anion exchange membrane water electrolyzers. *Energy Environ. Sci.* **2021**, *14*, 3393–3419. [[CrossRef](#)]
17. Igawa, M. Evolving Separation Techniques with Ion-Exchange Membranes. *Salt Seawater Sci.* **2021**, *1*, 1–9.
18. Khoiruddin, K.; Wardani, A.K.; Aryanti, P.T.; Wenten, I. Chapter 15—Polymeric membranes in electro dialysis, electro dialysis reversal, and capacitive deionization technologies. In *Advancement in Polymer-Based Membranes for Water Remediation*; Nayak, S.K., Dutta, K., Gohil, J.M., Eds.; Elsevier: Amsterdam, The Netherlands, 2022; pp. 541–567. [[CrossRef](#)]
19. Kamaroddin, M.F.A.; Sabli, N.; Abdullah, T.A.T.; Siajam, S.I.; Abdullah, L.C.; Jalil, A.A.; Ahmad, A. Membrane-based electrolysis for hydrogen production: A review. *Membranes* **2021**, *11*, 810. [[CrossRef](#)]
20. Shirvastian, P.; Loh, A.; Sluijter, S.; Li, X. Novel components in anion exchange membrane water electrolyzers (AEMWE's): Status, challenges and future needs. A mini review. *Electrochem. Commun.* **2021**, *132*, 107140. [[CrossRef](#)]
21. Chen, N.; Lee, Y.M. Anion exchange polyelectrolytes for membranes and ionomers. *Prog. Polym. Sci.* **2021**, *113*, 101345. [[CrossRef](#)]
22. Poźniak, G.; Trochimczuk, W. Interpolymer anion exchange membranes, I. Properties of weak base membranes based on polyethylene modified by styrene and divinylbenzene in the presence of diluents. *Die Angew. Makromol. Chem.* **1980**, *92*, 155–168. [[CrossRef](#)]
23. Gózdź, A.S.; Trochimczuk, W. Continuous modification of polyethylene with styrene and divinylbenzene in melt. *J. Appl. Polym. Sci.* **1980**, *25*, 947–950. [[CrossRef](#)]
24. He, Y.; Pan, J.; Wu, L.; Zhu, Y.; Ge, X.; Ran, J.; Yang, Z.; Xu, T. A Novel Methodology to Synthesize Highly Conductive Anion Exchange Membranes. *Sci. Rep.* **2015**, *5*, srep13417. [[CrossRef](#)] [[PubMed](#)]
25. Zhang, Y.; Parrondo, J.; Sankarasubramanian, S.; Ramani, V. Detection of Reactive Oxygen Species in Anion Exchange Membrane Fuel Cells using In Situ Fluorescence Spectroscopy. *Chemsuschem* **2017**, *10*, 3056–3062. [[CrossRef](#)] [[PubMed](#)]
26. Wang, G.; Weng, Y.; Chu, D.; Chen, R.; Xie, D. Developing a polysulfone-based alkaline anion exchange membrane for improved ionic conductivity. *J. Membr. Sci.* **2009**, *332*, 63–68. [[CrossRef](#)]
27. Couture, G.; Alaeddine, A.; Boschet, F.; Ameduri, B. Polymeric materials as anion-exchange membranes for alkaline fuel cells. *Prog. Polym. Sci.* **2011**, *36*, 1521–1557. [[CrossRef](#)]
28. Gu, S.; Cai, R.; Luo, T.; Chen, Z.; Sun, M.; Liu, Y.; He, G.; Yan, Y. A Soluble and Highly Conductive Ionomer for High-Performance Hydroxide Exchange Membrane Fuel Cells. *Angew. Chem. Int. Ed.* **2009**, *48*, 6499–6502. [[CrossRef](#)]
29. Merle, G.; Wessling, M.; Nijmeijer, K. Anion exchange membranes for alkaline fuel cells: A review. *J. Membr. Sci.* **2011**, *377*, 1–35. [[CrossRef](#)]
30. Ponce-González, J.; Ouachan, I.; Varcoe, J.R.; Whelligan, D.K. Radiation-induced grafting of a butyl-spacer styrenic monomer onto ETFE: The synthesis of the most alkali stable radiation-grafted anion-exchange membrane to date. *J. Mater. Chem. A* **2018**, *6*, 823–827. [[CrossRef](#)]
31. Wang, G.; Weng, Y.; Chu, D.; Xie, D.; Chen, R. Preparation of alkaline anion exchange membranes based on functional poly(ether-imide) polymers for potential fuel cell applications. *J. Membr. Sci.* **2009**, *326*, 4–8. [[CrossRef](#)]
32. Xiong, Y.; Liu, Q.L.; Zhu, A.M.; Huang, S.M.; Zeng, Q.H. Performance of organic–inorganic hybrid anion-exchange membranes for alkaline direct methanol fuel cells. *J. Power Sources* **2009**, *186*, 328–333. [[CrossRef](#)]
33. Jang, I.-Y.; Kweon, O.-H.; Kim, K.-E.; Hwang, G.-J.; Moon, S.-B.; Kang, A.-S. Application of polysulfone (PSf)– and polyether ether ketone (PEEK)–tungstophosphoric acid (TPA) composite membranes for water electrolysis. *J. Membr. Sci.* **2008**, *322*, 154–161. [[CrossRef](#)]

34. Ayaz, S.; Yao, Z.-Y.; Chen, Y.-J.; Yu, H.-Y. Preparation of poly(arylene ether ketone) based anion exchange membrane with pendant pyrimidinium and pyridinium cation derivatives for alkaline fuel cell. *J. Membr. Sci.* **2022**, *659*, 120778. [CrossRef]
35. Cha, M.S.; Park, J.E.; Kim, S.; Han, S.-H.; Shin, S.-H.; Yang, S.H.; Kim, T.-H.; Yu, D.M.; So, S.; Hong, Y.T.; et al. Poly(carbazole)-based anion-conducting materials with high performance and durability for energy conversion devices. *Energy Environ. Sci.* **2020**, *13*, 3633–3645. [CrossRef]
36. Pavel, C.C.; Cecconi, F.; Emiliani, C.; Santiccioli, S.; Scaffidi, A.; Catanorchi, S.; Comotti, M. Highly Efficient Platinum Group Metal Free Based Membrane-Electrode Assembly for Anion Exchange Membrane Water Electrolysis. *Angew. Chem. Int. Ed.* **2014**, *53*, 1378–1381. [CrossRef] [PubMed]
37. Faraj, M.; Boccia, M.; Miller, H.A.; Martini, F.; Borsacchi, S.; Geppi, M.; Pucci, A. New LDPE based anion-exchange membranes for alkaline solid polymeric electrolyte water electrolysis. *Int. J. Hydrog. Energy* **2012**, *37*, 14992–15002. [CrossRef]
38. Yee, R.; Rozendal, R.; Zhang, K.; Ladewig, B. Cost effective cation exchange membranes: A review. *Chem. Eng. Res. Des.* **2012**, *90*, 950–959. [CrossRef]
39. Henkensmeier, D.; Najibah, M.; Harms, C.; Žitka, J.; Hnát, J.; Bouzek, K. Overview: State-of-the Art Commercial Membranes for Anion Exchange Membrane Water Electrolysis. *J. Electrochem. Energy Convers. Storage* **2021**, *18*, 024001. [CrossRef]
40. Lim, A.; Kim, H.-J.; Henkensmeier, D.; Yoo, S.J.; Kim, J.Y.; Lee, S.Y.; Sung, Y.-E.; Jang, J.H.; Park, H.S. A study on electrode fabrication and operation variables affecting the performance of anion exchange membrane water electrolysis. *J. Ind. Eng. Chem.* **2019**, *76*, 410–418. [CrossRef]
41. Yan, X.; Yang, X.; Su, X.; Gao, L.; Zhao, J.; Hu, L.; Di, M.; Li, T.; Ruan, X.; He, G. Twisted ether-free polymer based alkaline membrane for high-performance water electrolysis. *J. Power Sources* **2020**, *480*, 228805. [CrossRef]
42. Varcoe, J.R.; Atanassov, P.; Dekel, D.R.; Herring, A.M.; Hickner, M.A.; Kohl, P.A.; Kucernak, A.R.; Mustain, W.E.; Nijmeijer, K.; Scott, K.; et al. Anion-exchange membranes in electrochemical energy systems. *Energy Environ. Sci.* **2014**, *7*, 3135–3191. [CrossRef]
43. Vincent, I.; Kruger, A.; Bessarabov, D. Development of efficient membrane electrode assembly for low cost hydrogen production by anion exchange membrane electrolysis. *Int. J. Hydrog. Energy* **2017**, *42*, 10752–10761. [CrossRef]
44. Masel, R.I.; Liu, Z.; Sajjad, S. Anion Exchange Membrane Electrolyzers Showing 1 A/cm<sup>2</sup> at Less Than 2 V. *ECS Trans.* **2016**, *75*, 1143. [CrossRef]
45. Gangrade, A.S.; Cassegrain, S.; Ghosh, P.C.; Holdcroft, S. Permselectivity of ionene-based, Aemion<sup>®</sup> anion exchange membranes. *J. Membr. Sci.* **2022**, *641*, 119917. [CrossRef]
46. Kang, S.Y.; Park, J.E.; Jang, G.Y.; Kim, O.-H.; Kwon, O.J.; Cho, Y.-H.; Sung, Y.-E. High-performance and durable water electrolysis using a highly conductive and stable anion-exchange membrane. *Int. J. Hydrogen Energy* **2022**, *47*, 9115–9126. [CrossRef]
47. Baldwin, R.S. A Review of State-of-the-Art Separator Materials for Advanced Lithium-Based Batteries for Future Aerospace Missions. 2009. Available online: <http://www.sti.nasa.gov> (accessed on 5 November 2022).
48. Tabani, Z.; Maghsoudi, H.; Zonouz, A.F. High electrochemical stability of polyvinylidene fluoride (PVDF) porous membranes using phase inversion methods for lithium-ion batteries. *J. Solid State Electrochem.* **2021**, *25*, 651–657. [CrossRef]
49. Alsabri, A.; Tahir, F.; Al-Ghamdi, S.G. Environmental impacts of polypropylene (PP) production and prospects of its recycling in the GCC region. *Mater. Today Proc.* **2022**, *56*, 2245–2251. [CrossRef]
50. Staño, L.; Stano, M.; Ďurina, P. Separators for alkaline water electrolysis prepared by plasma-initiated grafting of acrylic acid on microporous polypropylene membranes. *Int. J. Hydrog. Energy* **2020**, *45*, 80–93. [CrossRef]
51. Tsehaye, M.; Gebreslassie, G.T.; Choi, N.H.; Milian, D.; Martin, V.; Fischer, P.; Tübke, J.; El Kissi, N.; Donten, M.; Alloin, F.; et al. Pristine and Modified Porous Membranes for Zinc Slurry–Air Flow Battery. *Molecules* **2021**, *26*, 4062. [CrossRef]
52. Holda, A.K.; Vankelecom, I.F. Understanding and guiding the phase inversion process for synthesis of solvent resistant nanofiltration membranes. *J. Appl. Polym. Sci.* **2015**, *132*. [CrossRef]
53. Ion-Ebrasu, D.; Pollet, B.G.; Caprarescu, S.; Chitu, A.; Trusca, R.; Niculescu, V.; Gabor, R.; Carcadea, E.; Varlam, M.; Vasile, B.S. Graphene inclusion effect on anion-exchange membranes properties for alkaline water electrolyzers. *Int. J. Hydrog. Energy* **2020**, *45*, 17057–17066. [CrossRef]
54. Pozio, A.; Cemmi, A.; Carewska, M.; Paoletti, C.; Zaza, F. Characterization of gas diffusion electrodes for polymer electrolyte fuel cells. *J. Fuel Cell Sci. Technol.* **2010**, *7*, 0410031–0410037. [CrossRef]
55. Agel, E.; Bouet, J.; Fauvarque, J.F. Characterization and use of anionic membranes for alkaline fuel cells. *J. Power Sources* **2001**, *101*, 267–274. [CrossRef]
56. Kimura, T.; Yamazaki, Y. Effects of CO<sub>2</sub> Concentration and Electric Current on the Ionic Conductivity of Anion Exchange Membranes for Fuel Cells. *Electrochemistry* **2011**, *79*, 94–97. [CrossRef]
57. Ziv, N.; Dekel, D.R. A practical method for measuring the true hydroxide conductivity of anion exchange membranes. *Electrochem. Commun.* **2018**, *88*, 109–113. [CrossRef]
58. Ziv, N.; Mustain, W.E.; Dekel, D.R. The Effect of Ambient Carbon Dioxide on Anion-Exchange Membrane Fuel Cells. *Chemsuschem* **2018**, *11*, 1136–1150. [CrossRef]

**Disclaimer/Publisher’s Note:** The statements, opinions and data contained in all publications are solely those of the individual author(s) and contributor(s) and not of MDPI and/or the editor(s). MDPI and/or the editor(s) disclaim responsibility for any injury to people or property resulting from any ideas, methods, instructions or products referred to in the content.